ACS OMEGA

http://pubs.acs.org/journal/acsodf

Article

Experimental Study of the Formation Rate and Distribution of Methane Hydrate in Layered Sand

Yingmei Wang,* Shiqiang Dong,* Mengdi Zhang, Qingbai Wu, Xuemin Zhang, Peng Zhang, and Jing Zhan

Cite This: *ACS Omega* 2020, 5, 29882−29888

Read Online

ACCESS | Metrics & More | Article Recommendations

ABSTRACT: The geological structure and gas hydrate occurrence are stratification-dependent in the vertical direction. It is necessary to explore the formation processes and distribution characteristics of methane hydrate in layered porous media. The sand sample consists of two equal parts in a testing cylinder. The upper part is 0.5−1 mm sand in particle diameter, and the lower parts are 0.075∼0.5, 0.5∼1, and 1∼2 mm. The experimental results show that the formation rate of methane hydrate gradually decreases as the reaction goes on, and it is higher in layered sand than in nonlayered sand in the beginning. With the increase of the sand size in the lower part, saturation of methane hydrate gradually decreases in the upper part and increases in the lower part. In the layered sand, saturation of methane hydrate is higher in the sand layer whose particle size is bigger. The abovementioned results can be used to predict the favorable area where methane hydrate may appear in different stratigraphic structures in nature.

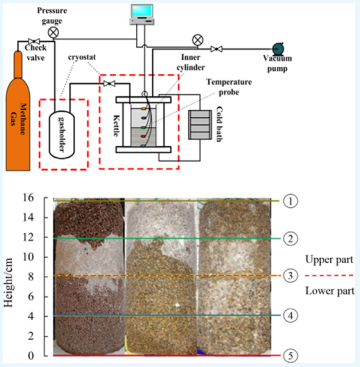

1. INTRODUCTION

Natural gas hydrate, which has a high resource density and burns cleanly,[1,2] is widely distributed in deep sea sediments and permafrost regions. The relevant research shows that as a type of natural resource, the reserve of the natural gas hydrate worldwide is twice as much as the fossil energy reserve. If rational mining is carried out, it could relieve the energy contradiction problem in the world.[3−5]

According to the geotechnical samples from the DK-2 borehole (Figure 1a), which were obtained in the frozen soil area of the Qilian Mountains,[6−8] methane hydrate is present in the interbed of the medium-to-fine sandstones at a depth of 144.4−152.0 m. The upper part of this interbed is a mixed sand layer, and the lower part is fractured oil shale. Hydrate is also present in the geological structure of silty mudstone with the oil shale interlayer at the depth of 235.0−291.3 m. The lithological composition in the deeper layer is medium sandstone. From the logging data in the Mallik area, Canada (3 L-38, 4 L-38, and 5 L-38), the gas hydrate[9] is distributed at the depth of 800−1100 m. The upper part is composed of small-size sand and is mixed with a small amount of mud shale, and the lower part is weakly consolidated siltstone and sandstone and siltstone with a large particle size (Figure 1b). The abovementioned results of drilling in the Qilian Mountains show that there are large differences in the vertical distribution of natural gas hydrate. The geological structure of its occurrence is stratification-dependent.[10] According to the drilling data, it can be seen that the hydrate may have different distributions in the layered sand sample with different sand sizes.

In recent years, many studies have focused on the effect of particle size on hydrate formation. In conclusion, there are three main types of opinions. The first opinion is that the large particle size is beneficial to hydrate formation in porous media because the water in the pores has high activity.[11−13] The second opinion is that small-size particles, which have a large specific surface area and can provide more nucleation points, can contribute to hydrate formation.[14−16] Pan reported that there is a critical size.[17] When the particle size is larger than this critical size, the sand with a larger particle size is conducive to hydrate formation. When the particle size is smaller than this critical size, the sand with a smaller particle size is conducive to hydrate formation.

In addition to particle size, water migration in the porous media is another important factor that affects hydrate formation. Temperature is one of three main factors that lead to water migration.[18] The water in porous media migrates from a high-temperature region to a low-temperature region.[19] When the soil freezes, the water moves toward the frozen fringe during the freezing process.[20] When there is a

Received: August 24, 2020
Accepted: October 28, 2020
Published: November 15, 2020

https://dx.doi.org/10.1021/acsomega.0c03984
ACS Omega 2020, 5, 29882−29888

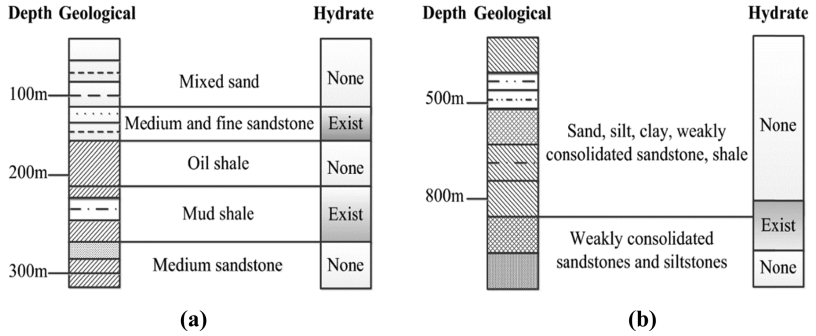

Figure 1. Drilling soil sample and hydrate distribution. (a) Permafrost of the Qilian Mountains and natural gas hydrate distribution and (b) permafrost of the Mallik areas and natural gas hydrate distribution.

temperature gradient in the soil, water migration will affect hydrate formation and distribution.[21−23] Compared to the uniform porous media, water migration in the layered media is different in the layered porous media.[24] Therefore, formation and distribution of gas hydrate in layered sand is different from that in nonlayered sand. This paper mainly focuses on the difference in the formation and distribution of methane hydrate in the layered and nonlayered porous media. The research can be expected to provide guidance for the survey of natural gas hydrate in unknown areas.

2. EXPERIMENTAL SECTION

2.1. Materials. The experimental device includes the gas supply system, experimental system, decomposition system, and data acquisition system (as shown in Figure 2), and the

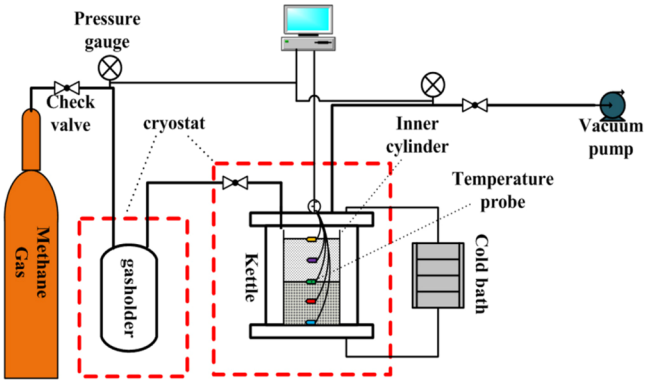

Figure 2. Schematic of the experimental system.

pressure range of the whole experimental system is −0.1 to 15.0 MPa. The gas supply system includes the gas source, pipeline, valve, and pressure gauge (range: 0.1−15.0 MPa; accuracy 0.25%). The experimental system includes the kettle (the inlet is at its top), inner cylinder, incubator, and JULABO cold bath made in Germany (temperature range—100−78 °C; accuracy ±0.01 °C). The decomposition system adopts the drainage method to collect the gas and measures the amount of gas obtained by decomposition with a measuring cylinder (Figure 3). The data-collecting system includes the Datataker acquisition instrument, computer, and temperature probes, which are made by the Northwest Institute of Eco-Environment and Resources, CAS, and uses the high-pressure and low-temperature thermistors (measuring range: 20−30 °C; accuracy ±0.05 °C).

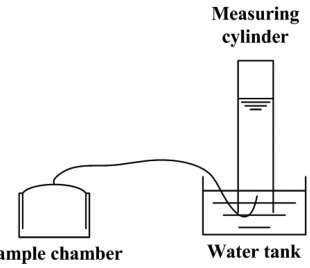

Figure 3. Decomposition and gas collection apparatus.

2.2. Experimental Methods. First, the tightness of the kettle and pipeline system was evaluated. Gas was charged into the kettle to 8.0 MPa, and if the pressure remained unchanged for 12 h, it implied that the whole system has a good tightness condition.

Second, samples were prepared. Five hundred grams of sand (see Table 1 for the parameters of the sand used) washed with

Table 1. Parameters of the Experimental Sand at the Same Volume

particle size (mm)	pore volume (cm^3/100 g)	quality (g)	water saturation (%)
0.075−0.5	24	500	50
0.5−1	33	500	50
1−2	35	500	50

distilled water was continuously dried in a drying oven for 12 h until it reached a constant weight. Distilled water was added to make the pore moisture content 50%. The mixture was stirred until it was uniform.

Third, the samples were loaded into the kettle. In the nonlayered sand sample, the upper and lower parts are 0.5−1 mm. In the layered sand sample, the upper part is 0.5−1 mm and the lower part is 0.075−0.5 or 1−2 mm in this paper (as shown in Figure 4). The temperature probes were placed at the center of the sand body at a distance of 4 cm from each other (as shown in the left of Figure 4). The sand samples had the same weight at the same height. Finally, the inner cylinder was placed into the kettle, and the kettle was sealed.

Fourth, the experiments were performed. The kettle was washed with methane gas three times after sealing the kettle. Then, the kettle was vacuumed for 20 min. Subsequently, the temperatures of the cold bath and the cryostat were adjusted, and then the whole kettle and sample was cooled down. When the temperature of the sand sample reached 0.5 °C and remained stable, the precooled methane gas in the gasholder

https://dx.doi.org/10.1021/acsomega.0c03984
ACS Omega 2020, 5, 29882−29888

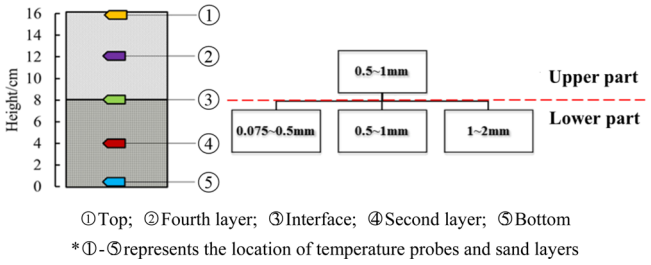

Figure 4. Position of temperature probes (left) and the sand layer (right). ①–⑤ represent the locations of temperature probes and sand layers. ① Top, ② fourth layer, ③ interface, ④ second layer, and ⑤ bottom.

(the gasholder in the cryostat, the temperature of which was set 0.5 °C too.) was charged into the kettle and stopped when the pressure reached 7.0 MPa (the inflation process took about 30 min). The time at which the pressure reached the established experimental condition was regarded as time zero. When the system pressure remained unchanged for 2 h, methane hydrate formation was considered to be over.

Fifth, the decomposition process was performed. To maintain the experimental distribution characteristics of methane hydrate in the kettle and reduce the experimental error caused by hydrate decomposition, the sand sample was quickly cooled to −8.0 °C and kept frozen for 12 h before the kettle was dismantled. Then, the kettle was opened, and the testing sand sample was taken photo. Then, the upper and lower parts were separated and placed in different sample chambers for decomposition (as shown in Figure 3) at the NPT condition, and the volume of methane gas was measured.

2.3. Calculations. The hydrate saturation and formation rates are calculated by the equations taken from the works by Wang[25] and Zhang,[26] respectively. This study mainly focuses on the amount of methane hydrate in the upper part and lower part and the characteristics of hydrate distribution in the layered media, and so, the perfect hydrate with the molecular formula $CH_4{\cdot}5.75H_2O$ is taken as the hydrate in this paper.

The volume of hydrate (V_h) is described as follows:

$$V_h = \frac{119.5}{16} \times \frac{\rho_0 V_0}{\rho_1}; \quad (1)$$

where 119.5 is the relative molecular mass of perfect methane hydrate, and 16 is the relative molecular mass of methane gas; ρ_0 is the density of methane gas, 0.716 g/L; V_0 is the volume of methane gas during decomposition, L; and ρ_1 is the density of methane hydrate, 0.91 g/cm^3.

All the pore volumes (V_k) of the sand sample in the upper or lower parts are described as follows:

$$V_k = \varphi \times 5; \quad (2)$$

where φ is the pore volume in every 100 g of sand in Table 1.

According to eqs 1 and 2, the hydrate saturation (S_h) is as follows:

$$S_h = \frac{V_h}{V_k}; \quad (3)$$

Methane gas consumption is described as follows:

$$\Delta n = \frac{P_1 V}{RT_1 Z_1} - \frac{P_2 V}{RT_2 Z_2}; \quad (4)$$

where V is the volume of gas in the kettle (about 1.04 L); P, T, and Z are the pressure, temperature, and gas compressibility factor at a certain point in time, respectively, and the hydrate formation rate (υ) is calculated as follows:

$$\upsilon = \frac{dV_h}{dt} = 119.5 \times \frac{\Delta n}{\Delta t}; \quad (5)$$

where V_h is the volume of methane hydrate, and Δn is the molar consumption of methane gas.

3. RESULTS AND DISCUSSION

3.1. Formation Process of Hydrate in the Layered Sand. *3.1.1. Changes in the Temperature and Pressure during the Formation of Methane Hydrate.* Figures 5 and 6 show the time-varying curves of temperature and pressure in the nonlayered sand sample and layered sand sample during the formation of methane hydrate, respectively. The temperature in the kettle rose rapidly because of the gas compression during the methane gas aeration. The temperature dropped down immediately after gas aeration, as shown in Figures 5 and 6. The orderly arranged water molecules need to break the bond of the surface energy of particles[27] during hydrate formation. There is a short supercooling phenomenon in the early stage of hydration formation, as shown in Figures 5 and 6.

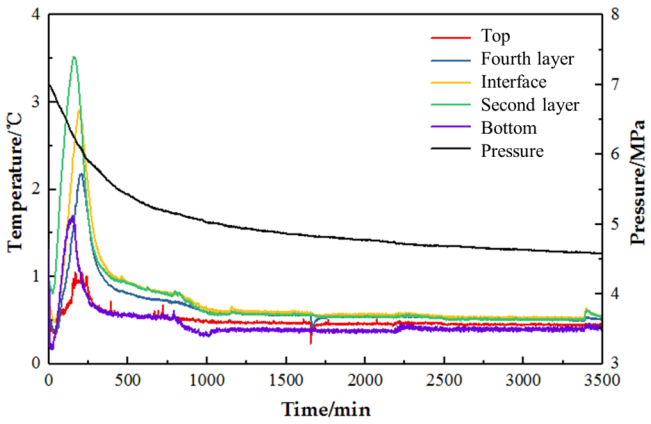

Figure 5. Time-varying curves of the temperature and pressure in nonlayered sand with 0.5−1 mm.

After the aeration, the temperatures of each layer in the sand rapidly decreased under the action of the cold bath and in the low-temperature box (Figure 5). Then, the temperature increased, and the pressure decreased. The analysis showed that a large amount of hydrate quickly formed at this time, which made the reaction heat[28] exceed the heat exchange capacity of the experimental system from the beginning to 250 min. The heat balance of this sand sample was broken, which quickly increased the temperature. When the reaction lasted for approximately 250 min, with the decrease in system pressure, increase in temperature, and decrease in water in the sand, the hydrate formation gradually slowed, the reaction heat gradually decreased, and the temperature of each layer began to decline. During the period of 400−1000 min in this experiment, the temperature was slightly higher than the equilibrium temperature in the fourth layer, interface, and second layer. The hydrate formation rate was still slow at this time. When the temperatures of each layer reached the equilibrium temperature after 1000 min, the hydrate formation process became very slow.

https://dx.doi.org/10.1021/acsomega.0c03984
ACS Omega 2020, 5, 29882−29888

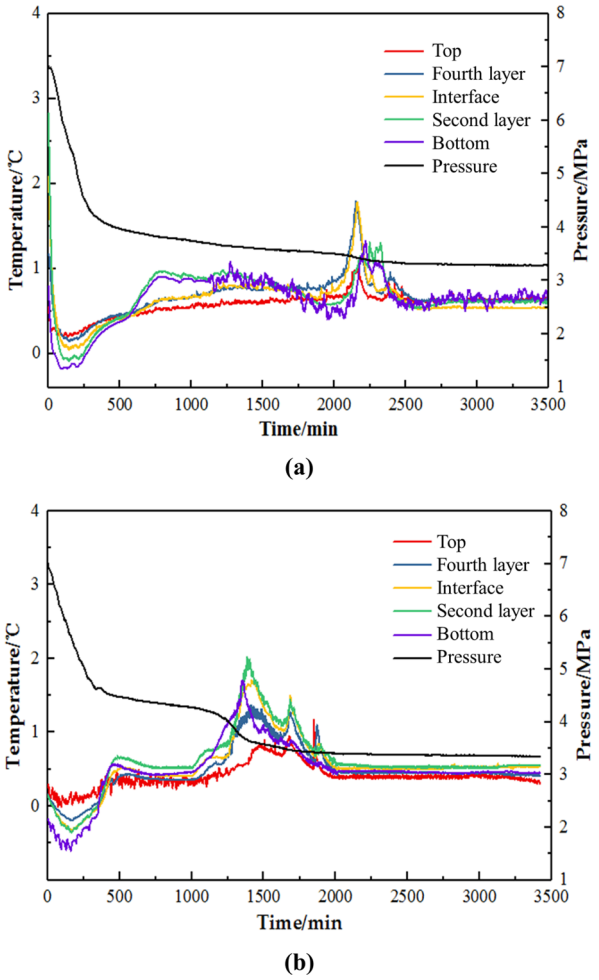

Figure 6. Hydrate formed in layered sand samples. (a) Time-varying curves of the temperature and pressure in sand with particle sizes of 0.075−0.5 mm as the lower part. (b) Time-varying curves of the temperature and pressure in sand with particle sizes of 1−2 mm as the lower part.

In nonlayered sand, the cooling method was simultaneously applied at both ends in this experiment. When no hydrate is formed, the temperature sequence of those five layers should be as follows: the top and bottom, followed by the second and fourth layers, and interface in approximately 250 min. However, in this nonlayered sand sample, the sequence of temperature peaks is as follows: second layer, interface, fourth layer, top, and bottom. It means that the hydrate formed in the second layer is maximum, followed by the interface, fourth layer, top, and bottom at that moment. Also, hydrates in the bottom and second layers formed first, then in the top and fourth layers, and finally at the interface, as shown in Figure 5. The reason was that the hydrate in the upper part gradually blocked the pores, which hindered the full contact between gas and water in the lower part. The upper part can obtain sufficient gas supply at this time, there was enough hydrate formed in the upper part,[21] and the temperature increased.

Figure 6 shows the time-varying curves of temperature and pressure in the layered sand in the experiment. Figure 6a shows the time-varying curves of temperature and pressure in the sand that has a lower part with a particle size of 0.075−0.5 mm, and Figure 6b shows the time-varying curves of temperature and pressure in the sand that has a lower part with a particle size of 1−2 mm. In Figure 6, the hydrate formation processes in the layered sand samples are similar. According to the changes of temperature and pressure with time in the experiment, hydrate formation can be roughly divided into four stages. In the first stage of hydrate formation, the temperature and pressure began to decrease (0−150 min) after inflation; then, the temperature began to increase at approximately 150 min. At this time, hydrate began to form, which made the temperature to increase and the pressure to rapidly decrease. Then, the hydrate formation went into the second stage. The temperature stabilized at approximately the experimental temperature in 750−1900 min (Figure 6a) and 500−1000 min (Figure 6b), while the pressure still slowly decreased. There are two main reasons: the hydrate formation first occurred on the contact surface between the surface of the sand sample and the inner cylinder wall,[5] which had a weak "armor effect[29]" and hindered the full contact between water and gas to form a large amount of hydrate. The second reason is that the hydrate formation in the sand sample was relatively slow, so the temperature did not significantly increase. Then, the hydrate formation entered the third stage, where the temperature sharply increased and the pressure rapidly decreased at approximately 1900 and 1000 min. At this stage, hydrate mainly formed in the interior of the "armor", and the gas gradually penetrated into the interior of the "armor". The "armor" slowly thickened and grew toward the center of the sand sample. After a while, hydrates began to form in large quantities in the sand sample. Finally, the reaction entered the fourth stage of hydrate formation, where the pressure and temperature gradually became stable (Figure 6a: 2600 min—end of the experiment; Figure 6b 2000 min—end of the experiment). With gas consumption in this stage, hydrate formation gradually slowed until the end.

The decreases in pressure in the two-layered sand samples are very similar, which indicates that the initial pressure has little effect on the final conversion rate of hydrates in the layered sand sample. The decrease in pressure is significantly larger in the layered sand sample than in the nonlayered sand sample. Thus, the layered sand sample may be conducive to improving the final conversion rate of hydrates than the nonlayered sand sample.

3.1.2. Formation Rate of Methane Hydrates in Different Sand Samples. When the temperature and pressure data are added to formula 5, the hydrate formation rate in different sand samples changes with time (as shown in Figure 7). After inflation, the hydrate began to form in large quantities, and the hydrate formation rate is the largest. As the reaction proceeded, the hydrate formation rate gradually decreased. In contrast, the hydrate formation rate in the nonlayered sand decreased less than in the layered sand. In the early stage (0−300 min) of the hydrate formation process, the formation rates of this two-layered sand samples were higher than those in the nonlayered sand. When the reaction lasted for 300 min, the formation rate in the layered sand samples became lower than that in the nonlayered sand. There was only one peak in the beginning of the whole formation process in the nonlayered sand, while there were two obvious peaks in the layered sand. In total, the reaction lasted for approximately 2000 min; for the layered sand with a particle size of 0.075−0.5 mm as the lower part, its formation rate slightly increased until the second peak appeared, and it began to gradually decline for approximately 100 min until the reaction ended. In the sand sample with a particle size of 1−2 mm as the lower part, the reaction lasted

https://dx.doi.org/10.1021/acsomega.0c03984
ACS Omega 2020, 5, 29882−29888

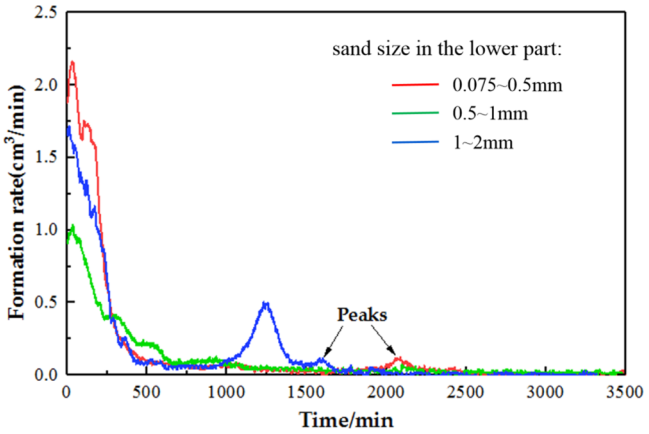

Figure 7. Variations in the hydrate formation rate in different sand samples with different sand sizes as the lower part (red line: upper part is 0.5−1 mm, lower part is 0.075−0.5 mm; light green: nonlayered sand sample; blue line: upper part is 0.5−1 mm, lower part is 1−2 mm)

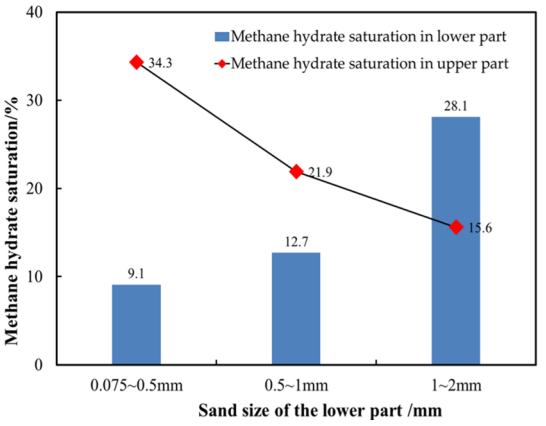

Figure 8. Methane hydrate saturation in the upper and lower parts (the red diamond points represent hydrate saturation in upper parts with 0.5−1 mm; the blue rectangular columns represent hydrate saturation in lower parts with different sand sizes).

for approximately 1000 min. The reaction has a large increase range and a long duration. After 500 min, the formation rate began to gradually decrease; then, some small peaks appeared. The hydrate formation rate in every sand sample gradually decreased until the hydrate formation rate was stable. Because a larger pore size has a larger particle size, more time is required from when hydrates begin to form the crystal nucleus to when the pore is completely filled for a particle with a small pore size. Therefore, methane gas takes longer to penetrate the sand sample and combine with water to form hydrates. Gas is transported through the internal channel of the sand sample with a larger particle size. The second peak value of the velocity in the sand sample with the large-particle-size lower part lasts longer than that in the sand sample with the small-particle-size lower part.

3.2. Saturation and Distribution of Methane Hydrate in Different Sand Samples. Methane hydrate saturation is the ratio of the volume of methane hydrate to the total pore volume in the porous medium.[30] On adding the volume of methane gas during decomposition to formula 3, hydrate saturation in the upper and lower parts can be calculated (as shown in Figure 8). Migration of water under the capillary force and permeability in porous media contributed to hydrate formation in the sand samples, which has obvious stratification characteristics.

From hydrate saturation in the upper part and lower part, as shown in Figure 8, it can be seen that when the lower part of the sand has the smallest particle size (0.075~0.5 mm), hydrate saturation in the upper part is maximum (approximately 34.3%) and hydrate saturation in the lower part is minimum, only 9.1%. When the particle size of the lower part changed to 1~2 mm, hydrate saturation in the upper part is minimum, about 15.6%, and it is maximum in the lower part, about 28.1%. According to the variation trend, hydrate saturation gradually decreased in the upper part and increased in the lower part, with the particle size of the lower part increased in a certain particle size range.

It was found that the layered sand, according to hydrate saturation in the upper part and lower part in the overall layered sand sample, has higher hydrate saturation in the part which has a larger particle size. According to the Kozeny−Carman equation,[31] the permeability k in the porous media is $k = \frac{r^2\varphi^3}{180(1-\varphi)^3}$; where r is the aperture and φ is the porosity of sand. It can be seen that they have a better permeability and better water activated in the sand layer which has a larger size, so the methane gas has a favorable contact with water in the sand, which results in hydrate saturation in the sand with a larger particle size being larger than that in the sand with a smaller particle size.

In the nonlayered sand (0.5−1 mm sand as the lower part), the hydrate formed in the upper part blocked the pores, and the methane gas has no better contact with water which is in the lower part, and so, hydrate saturation in the upper part is greater than that in the lower part.

Figures 8 and 9 show that hydrate distribution is similar to the saturation of hydrates calculated by the decomposition in the upper and lower parts.

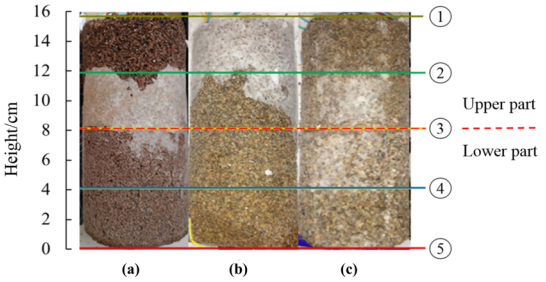

Figure 9. Hydrate distribution patterns in the surface of different sand samples. (a) Lower part is 0.075−0.5 mm; (b) lower part is 0.5−1 mm; and (c) lower part is 1−2 mm.

From the Figure 9, it can be seen that the formed hydrate is concentrated near the interface on the surface of the layered sands (Figure 9a,c). For the layered sand sample with 0.075−0.5 mm as the lower part, the hydrate is mainly distributed on the surface between the interface and the fourth layer in large quantities, and it is film-like on the surface of the lower part. Although the hydrate is visible among the sand particles with a particle size of 1−2 mm in the lower part, there are significantly more hydrates between the second layer and fourth layer than in the remaining layers. The reason is that the permeability coefficient of the sand with a larger size is much higher than that of the sand with a smaller size.[32] Therefore, it

https://dx.doi.org/10.1021/acsomega.0c03984
ACS Omega 2020, 5, 29882−29888

is harder for methane gas to permeate into the lower part where the sand is of 0.075−0.5 mm in size, resulting in the distribution of hydrates in the layered sand with a particle size of 0.075−0.5 mm as the lower part. However, it has a better permeability in the layered sand with a particle size of 1−2 mm as the lower part, and then the hydrate can grow in the lower part. Moreover, the soil matrix potential near the boundary can be abrupt, so the water retention was near the junction of two sand layers.

In the semisaturated layered sand samples, water migrated toward the junction between two interfaces. The amount of water increased when the hydrate gradually thickened from the contact surface between the sand sample and the inner cylinder to the center of sand.[33]

However, in the nonlayered sand (Figure 9b), the hydrate is mainly distributed on the surface of the top of sand in large quantities. Methane gas permeates into the sand body when it is charged into the kettle. During the hydrate formation, the pore is blocked by the hydrate, and it is hard for methane gas to permeate into the lower part, but it has a better contact with methane gas on the top of the sand, and so, the hydrate grows better on the top of the sand. Finally, Figure 9 shows the distribution and morphology of methane hydrate on the surface of quartz sand, and the distribution of methane hydrate is mainly based on saturation calculation results.

4. CONCLUSIONS

In the quartz sand with a particle size range of 0.075−2 mm, when the 0.5−1.0 mm sand is used as the upper part and sand with particle sizes of 0.075−0.5, 0.5−1, and 1−2 mm is used as the lower parts to form a bistratal sand, methane hydrate is formed by the pressure reducing method. The results show that within a certain particle size range, the formation process and hydrate distribution are quite different in the nonlayered sand sample and layered sand sample. Two rapid formation stages appear in the layered sand sample because of the "armor." Hydrate saturation in the upper part increases with the decrease in the particle size of the lower parts, while the hydrate saturation decreases in the lower part. In addition, the photographs show that the hydrate-rich area in the layered sand is different from that in the nonlayered sand. The hydrates are enriched in the junction because of the retention effect of water near the junction in the layered sand. However, in the nonlayered sand, the hydrate is mainly concentrated near the top of the nonlayered sand sample. It can be predicted that the hydrate accumulation near the junction of two interfaces in stratified strata might be substantial in nature and the top of the nonlayered strata might be enriched.

AUTHOR INFORMATION

Corresponding Authors

Yingmei Wang − *School of Energy and Power Engineering, Lanzhou University of Technology, Lanzhou 730050, China; Key Lab of Complementary Energy System of Biomass and Solar Energy Gansu Province, Lanzhou 730050, China; Collaborative Innovation Center of Key Technology for Northwest Low Carbon Urbanization, Lanzhou 730050, China*; Email: wymch@lzb.ac.cn

Shiqiang Dong − *School of Energy and Power Engineering, Lanzhou University of Technology, Lanzhou 730050, China; Key Lab of Complementary Energy System of Biomass and Solar Energy Gansu Province, Lanzhou 730050, China; Collaborative Innovation Center of Key Technology for Northwest Low Carbon Urbanization, Lanzhou 730050, China*; orcid.org/0000-0002-2803-4371; Email: sq.dong@qq.com

Authors

Mengdi Zhang − *School of Energy and Power Engineering, Lanzhou University of Technology, Lanzhou 730050, China; Key Lab of Complementary Energy System of Biomass and Solar Energy Gansu Province, Lanzhou 730050, China; Collaborative Innovation Center of Key Technology for Northwest Low Carbon Urbanization, Lanzhou 730050, China*

Qingbai Wu − *State Key Laboratory of Frozen Soil Engineering, Northwest Institute of Eco-Environment and Resources, CAS, Lanzhou 730000, China*

Xuemin Zhang − *School of Energy and Power Engineering, Lanzhou University of Technology, Lanzhou 730050, China; Key Lab of Complementary Energy System of Biomass and Solar Energy Gansu Province, Lanzhou 730050, China; Collaborative Innovation Center of Key Technology for Northwest Low Carbon Urbanization, Lanzhou 730050, China*; orcid.org/0000-0002-4054-0007

Peng Zhang − *State Key Laboratory of Frozen Soil Engineering, Northwest Institute of Eco-Environment and Resources, CAS, Lanzhou 730000, China*; orcid.org/0000-0003-3367-977X

Jing Zhan − *State Key Laboratory of Frozen Soil Engineering, Northwest Institute of Eco-Environment and Resources, CAS, Lanzhou 730000, China*

Complete contact information is available at: https://pubs.acs.org/10.1021/acsomega.0c03984

Notes

The authors declare no competing financial interest.

ACKNOWLEDGMENTS

This work was supported by National Natural Science Foundation of China (NO: 41661103); National key R & D projects (NO: 2017YFC0307303); Open fund of National Key Laboratory of frozen soil engineering, CAS (NO: SKLFSE201406), and National Natural Science Foundation of China (NO: 51906093). Professor Yibin Pu is thanked for the help provided to set up the experiment platform.

REFERENCES

(1) Babu, P.; Yee, D.; Linga, P.; Palmer, A.; Khoo, B. C.; Tan, T. S.; Rangsunvigit, P. Morphology of methane hydrate formation in porous media. *Energy Fuels* **2013**, *27*, 3364−3372.

(2) Sloan, E. D. Fundamental principles and applications of natural gas hydrates. *Nature* **2003**, *426*, 353−359.

(3) Zhao, Z. B.; Qiu, X. Q.; Xu, J. L. Finite element analysis of modal vibrations of drill strings in deep-sea natural gas hydrate coring/drilling. *Nat. Gas Ind.* **2011**, *31*, 73−76.

(4) Wang, Z. F.; Guan, Z. C.; Xu, J. L. Research and development of a gas hydrate coring system in the deep seawater. *Nat. Gas Ind.* **2012**, *32*, 46−48.

(5) Liang, D. Q.; Zang, X. Y.; Wu, N. Y. A simulation study of natural gas hydrate generation in mesoscopic-scale pores. *Nat. Gas Ind.* **2013**, *33*, 24−28.

(6) Lu, Z. Q.; Zhu, Y. H.; Zhang, Y. Q.; Wen, H. J.; Li, Y. H.; Jia, Z. Y.; Liu, C. L.; Wang, P. K.; Li, Q. H. Basic geological characteristics of gas hydrate in Qilian Mountain permafrost area. *Qinghai Province. Miner. Depos.* **2010**, *29*, 182−191.

(7) Zhang, P. H.; Fang, H.; Bai, D. W.; He, M. X.; Lv, Q. Y. Reservoir characteristics of gas hydrate in the Muli permafrost region. *J. Northeast Pet. Univ.* **2018**, *42*, 122−123.
(8) Wang, W. C.; Lu, Z. Q.; Li, Y. H.; Zhang, W. L.; Liu, W. J.; Li, X. Distribution and reservoir characteristics of gas hydrates in Sanlutian of Muli, Qinghai. *Geoscience* **2015**, *29*, 1035−1046.
(9) Tomaru, H.; Fehn, U.; Lu, Z.; Matsumoto, R. Halogen systematics in the Mallik 5L-38 gas hydrate production research well, Northwest Territories, Canada: Implications for the origin of gas hydrates under terrestrial permafrost conditions. *Appl. Geochem.* **2007**, *22*, 656−675.
(10) Dallimore, S.R.; Collett, T.S. Scientific Results from the Mallik 2002 Gas Hydrate Production Research Well Program, Mackenzie Delta, Northwest Territories, *Canada. Bull. Geol. Surv. Can.* 2005, *585*, DOI: 10.4095/220702.
(11) Chong, Z. R.; Yang, M. J.; Khoo, B. C.; Linga, P. Size effect of porous media on methane hydrate formation and dissociation in an excess gas environment. *Ind. Eng. Chem. Res.* **2016**, *55*, 7981−7991.
(12) Sun, S. C.; Liu, C. L.; Ye, Y. G.; Liu, Y. F. Phase behavior of methane hydrate in silica sand. *J. Chem. Thermodyn.* **2014**, *69*, 118−124.
(13) Liu, W.; Wang, S.; Yang, M.; Song, Y.; Wang, S.; Zhao, J. Investigation of the induction time for THF hydrate formation in porous media. *J. Nat. Gas Sci. Eng.* **2015**, *24*, 357−364.
(14) Zhao, J.; Lv, Q.; Li, Y.; Yang, M.; Liu, W.; Yao, L.; Wang, S.; Zhang, Y.; Song, Y. In-situ visual observation for the formation and dissociation of methane hydrates in porous media by magnetic resonance imaging. *Magn. Reson. Imaging* **2015**, *33*, 485−490.
(15) Li, M. C.; Fan, S. S.; Zhao, J. Z. Experimental study on formation of natural gas hydrate in porous media. *Nat. Gas Ind.* **2006**, 27−28.
(16) Bagherzadeh, S. A.; Moudrakovski, I. L.; Ripmeester, J. A.; Englezos, P. Magnetic resonance imaging of gas hydrate formation in a bed of silica sand particles. *Energy Fuels* **2011**, *25*, 3083−3092.
(17) Pan, Z.; Liu, Z. M.; Liu, D. J.; Shang, L. Y.; Li, W. Z.; Li, P. Research progress on influence factors of natural gas hydrate formation in porous media. *Chem. Ind. Eng. Prog.* **2017**, *36*, 4403−4415.
(18) Xu, X.Z.; Deng, Y.S. *Experimental study on water migration in freezing and frozen soils*, 1st ed.; Science Press: Beijing, China, 1991; pp. 13.
(19) Fu, Q.; Hou, R. J.; Li, T. X.; Ms, Z. A.; Peng, L. Soil moisture-heat transfer and its action mechanism of freezing and thawing soil. *Trans. Chin. Soc. Agri. Machine.* **2016**, *47*, 99−110.
(20) Bronfenbrener, L.; Bronfenbrener, R.; Alafenish, A. A model of soils freezing with allowance for freezing zone. *Chem. Eng. Process.: Process Intesif.* **2013**, *73*, 38−49.
(21) Wang, Y. M.; Wu, Q. B.; Jiang, G. L. Effect of temperature gradient on process of methane hydrate formation in non-saturated coarse sand. *J. Central South Univ. Sci. Technol.* **2014**, *45*, 507−514.
(22) Zhang, P.; Wu, Q. B.; Wang, Y. M. Water transfer rules during methane hydrate formation and dissociation inside saturated coarse sand and loess. *Chin. J. Geophys.* **2011**, *54*, 1071−1078.
(23) Zhang, P.; Wu, Q. B.; Wang, Y. M. Water change characteristics of formation and dissociation of methane hydrate in non-saturated media. *Prog. Geophys.* **2010**, *25*, 1339−1345.
(24) Song, C. Water movement in unsaturated layered soil under constant waterhead. Chengdu University of Technology, 2014.
(25) Wang, Y. M.; Wu, Q. B.; Pu, Y. B.; Zhan, J. Effect of temperature gradient on process of methane hydrate formation-dissociation and its resistivity changes in coarse sand. *Nat. Gas Geosci.* **2012**, *23*, 19−25.
(26) Zhang, Y.; Wu, H. J.; Li, X. S.; Li, G.; Chen, Z. Y.; Zeng, Z. Y. Experimental study on formation behavior of methane hydrate in porous media. *Acta Chim. Sin.* **2011**, *69*, 2221−2227.
(27) Xu, X.Z.; Wang, J.C.; Zhang, L.X. *Permafrost Physics*, 1st ed.; Science Press: Beijing, China, 2001; pp. 112−113.
(28) Chen, W. S.; Li, Z. H.; Wu, Q. Experimental study of the relationship between temperature field distribution of methane hydrate formation process and the formation rate. *J. Chin. Coal Soc.* **2015**, *40*, 1065−1069.
(29) Chen, L.; Zhang, Y.; Li, X. S.; Chen, Z. Y.; Li, G. Experimental study of methane hydrate formation in quartz media. *Nat. Gas Chem. Ind.* **2018**, *43*, 60−66.
(30) Yousif, M.H. The kinetics of hydrate formation. *SPE Annual Technical Conference and Exhibition*, 1994, *11*, 452−458.
(31) Kozeny, J. Uber die kapillare Leitung des Wassers im Boden[J]. *Sitzungsber. Akad. Wiss.* **1927**, *136*, 271−306.
(32) Dai, S.; Seol, Y. Water permeability in hydrate-bearing sediments: A pore-scale study. *Geophys. Res. Lett.* **2014**, *41*, 4176−4184.
(33) Hill, D. E.; Parlange, J. Y. Wetting front instability in layered soils. *Soil Sci. Soc. Am. J.* **1972**, *36*, 697−702.

https://dx.doi.org/10.1021/acsomega.0c03984
ACS Omega 2020, 5, 29882−29888